Eurographics Conference on Visualization (EuroVis) 2013
B. Preim, P. Rheingans, and H. Theisel
(Guest Editors)

Volume 32 (2013), Number 3

Mass-Dependent Integral Curves in Unsteady Vector Fields

Tobias Günther[1] Alexander Kuhn[2] Benjamin Kutz[3] Holger Theisel[1]

[1]Visual Computing Group, University of Magdeburg
[2]Visualization and Data Analysis, Zuse Institute Berlin
[3]Institute of Aerodynamics and Gas Dynamics, University of Stuttgart

Abstract

Recent research in flow visualization is focusing on the analysis of time-dependent, but mass-less particles. However, in many application scenarios, the mass of particles – and their resulting inertia – is essential in understanding fluid mechanics. This includes critical processes, such as dust particles interacting with aircraft (e.g., brown- or white-out effects) and particle separation based on density variation. In this paper, we contribute a generalized description of mass-dependent particle trajectories and apply existing unsteady flow visualization methods to the mass-dependent case. This comprises the extension of common concepts, i.e., path lines, streak lines, and time lines. Furthermore, we introduce a new class of integral curves, called mass lines that effectively visualizes mass separation and captures mass-related features in unsteady flow fields that are inaccessible using traditional methods. We demonstrate the applicability of our method, using a number of real-world and artificial data sets, in which mass is a crucial parameter. In particular, we focus on the analysis of brown-out conditions, introduced by a helicopter in forward flight close to the ground.

This is the authors preprint.
The definitive version of the paper is available at http://diglib.eg.org/ and http://onlinelibrary.wiley.com/.

1. Introduction

Particle-based flow visualization has a long tradition in experimental and computational fluid dynamics, cf. McLoughlin et al. [MLP*09]. So far, the flow visualization literature only used mass-less particles, since the tangent of their trajectory directly correlates to the velocity direction in the vector field, making mass-less particles a meaningful tool to visualize the vector field. In many applications, however, the trajectory of mass-dependent particles is of interest, not the underlying vector field. The behavior of such particles differs notably from infinitesimal particle dynamics, cf. Haller and Sapsis [HS08]. The equations of motion, defining the behavior of the particles, need to be modeled according to the assumptions made in the respective application. In order to generalize this we introduce a unified visualization framework for the geometry-based analysis of mass-dependent particles. This paper provides the following contributions:

- A unified description of mass-dependent particle trajectories independent of the application case, i.e., mass-dependent path lines.
- In order to reveal temporal and spatial coherent structures, we derive mass-dependent streak lines and time lines.
- To analyze the influence of the mass on the trajectories, a new class of integral lines is introduced, called *mass lines*.
- We demonstrate the utility of mass-dependent geometric flow visualization tools by the example of interactive brown-out simulations on the GPU.

The applications of mass-dependent particle visualizations are numerous and of great importance, e.g., in understanding particle seperation due to density variations (for instance by hydrocyclones), or the analysis of the aerodynamics around a helicopter close to the ground, which is our primary example. When approaching the ground or hovering near it, the aerodynamics around a helicopter is significantly altered compared to the free flight. Especially the wake of the rotor is influenced, hindered and deflected by the ground. This flow regime is known to be highly unsteady and three-dimensional. Therefore, not all the mechanisms are fully understood [SGL10]. When this flight state occurs over a terrain with loose ground, such as sand or snow, the wake will lift up sediment particles, which will be entrained into the surrounding flow of the helicopter and lead to a dangerously obscured view capability of the pilot. This phenomenon is

known as brown- or white-out and may be hazardous to the flight crew as well as the ground personnel [MKW08].

2. Related Work

In this section we outline recent work on mass-less particle-based flow visualization, integration of mass-dependent particles and observations of aerodynamics around helicopters.

2.1. Mass-less Particle-based Flow Visualization

Most flow visualization techniques rely on virtual mass-less particles moving within the underlying flow field. A system for the interactive visualization of large particle sets, exploiting graphics hardware capabilities, is presented by Krüger et al. [KKKW05] and another system to explore multi-variate flow properties is presented by Fraedrich and Westermann [FW12]. In addition, GPU realizations for massive particle advection in steady and time-dependent vector fields have been presented by Peterka et al. [PRN*11], Kipfer et al. [KSW04] and Hlawatsch et al. [HSW11].

In general, direct particle visualization does only allow for limited insight into the dynamic motion behavior. Hence, a common approach is the usage of integral geometry, based on the trajectories of moving particles, to visualize their long-term behavior and structural patterns therein. Dependent on the spatio-temporal context, characteristic curves can be defined, such as stream lines, path lines, streak lines, and time lines. A profound overview of integral geometry approaches is given by McLoughlin et al. [MLP*09]. Streak lines, time lines and integral surfaces additionally capture the behavior of neighboring flow particles across the temporal and/or spatial domain. This spatio-temporal connection requires adaptive refinement to be resolved over longer observation times (see e.g., [WWSS10] or [BFTW09] for streak surfaces). Recently, Weinkauf et al. [WHT12] proposed a generalized scheme to describe any time-dependent curve type by means of a stream line integration of a derived higher-order vector field. The advection of additional flow field properties along particle trajectories, further allows to derive insight into the dynamics of those properties. Li et al. [LTH08] propose a physically oriented dye advection scheme using mass conservation, which was later improved by Karch et al. [KSW*12].

2.2. Mass-dependent Particle Integration

Up to now, all presented approaches rely on trajectories of mass-less particles moving within the flow field. Physical parameters, such as density or particle size, can only be considered in post processing of the mass-independent trajectories. However, in many applications, the mass of transported particles, and resulting inertia, has critical impact to observable phenomena and are yet inaccessible to the previous methods. The consideration of particle mass has fundamental implications on the numerical integration process, as a number of forces acts on finite-size particles in viscous fluids. This includes the force exerted by flow itself (a), buoyancy force (b), Stokes drag (c), force exerted due to mass of fluid moving with the particle (d) and the Basset-Boussinesq memory term (e) (see Haller and Sapsis [HS08]). Dependent on the application case, several forces can be neglected. Haller and Sapsis [HS08] for instance, derive a model for very small particles in unsteady flows, neglecting the terms (c), (d) and (e). Further assuming that the particles have a much higher density than the carrying fluid (e.g., dust or sand in air), the buoyancy force (b) further simplifies to the model of Crowe et al. [CST98], which is used and explained later on in Section 3.2. The effect of inertia, resulting from finite-sized particles, has been studied by Cartwright et al. [CFK*10]. The motion dynamics of dust particles with mass in vortical flows has been analyzed by Angilella [Ang10].

2.3. Aerodynamics around Helicopters

One specific application in which particle mass is crucial, are so called brown-out (in case of dust or sand) or white-out (in case of snow) effects during helicopter flight. Since both aspects are highly relevant for safety and aerodynamically challenging, a great amount of theoretical, experimental and computational work has been done on this topic. Theoretical examinations have been presented by Betz [Bet37], Heyson [Hey60], and Fradenburgh [Fra59], which introduced models to reproduce the effect of ground on a helicopter. Based on this, several experimental correlations and empirical models have been introduced and validated [Zbr47, SGHK03, LLR08, NG12]. With increasing computational power and effectiveness of computational methods the impact of the ground on the aerodynamics of the helicopter could be analyzed in a purely numerical setup. Computational methods used for this flight state can be divided into finite state modeling (Xin et al. [XPP00]), free vortex/ potential models (D'Andrea [D'A10]) and Euler-/ Navier Stokes methods (Kalra et al. [KLB10]). A profound summary of the described effects are listed in PhD theses by Nathan [Nat10], Pulla [Pul06], and Ganesh [Gan06]. In addition to this, Syal et al. [SGL10] presented a detailed overview of brown-out particle modeling, which will be subject to a more detailed discussion in Section 3.2.

3. Mass-dependent Particles

In this section, we introduce a generalized description of mass-dependent particles and elaborate on one particular particle model, used for brown-out simulations.

3.1. Mass-dependent Flow Map

Given is a 3D time-dependent vector field $\mathbf{u}(\mathbf{x},t)$. For simplifying explanations we assume its domain – both spatial and temporal – to be infinite, which ensures that the integration

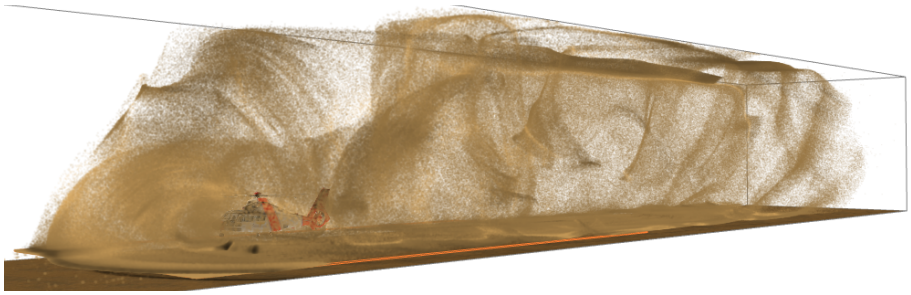

Figure 1: *Interactive simulation of brown-out conditions, encountered by a helicopter in forward flight close to the ground.*

of $\mathbf{u}$ never leaves the domain. (In real data sets, a boundary treatment is necessary.) In order to decouple the derivation of integral curves from the particle model, we generalize the particle model by extending the concept of *flow map* ϕ (cf. [Sha05]) to mass-dependent particles. This yields a new mass-dependent flow map $\phi_t^\tau(\mathbf{x}, r, \mathbf{v}_0)$ that describes where a particle with response time r, seeded at location $(\mathbf{x}, t)$, and with an initial velocity $\mathbf{v}_0$ moves to during integration of $\mathbf{u}$ over a time interval τ. The particle response time r depends on a number of particle characteristics, such as mass, size and viscosity, and is explained later in Section 3.2. The mass-dependent flow map can be understood as a black-box, comprising the application-dependent equations of motion.

In the remainder of this paper we consider all particles to be released from rest. For brevity we therefore shortly denote the mass-dependent flow map for particles released from rest as $\phi_t^\tau(\mathbf{x}, r)$. Note that mass-dependent particles develop inertia, which influences the trajectory. In contrast to the classic flow map, the following property therefore does not generally hold in the shortened notation, as the velocity of the particle is assumed to be zero at time $t + \tau_1$:

$$\phi_{t+\tau_1}^{\tau_2}(\phi_t^{\tau_1}(\mathbf{x}, r), r) \neq \phi_t^{\tau_1+\tau_2}(\mathbf{x}, r).$$

The property, however, is fullfilled by considering the initial velocity when continuing the integration, as in the unshortened description:

$$\phi_{t+\tau_1}^{\tau_2}(\phi_t^{\tau_1}(\mathbf{x}, r, \mathbf{v}_0), r, \frac{\mathrm{d}\phi_t^{\tau_1}}{\mathrm{d}\tau}(\mathbf{x}, r, \mathbf{v}_0)) = \phi_t^{\tau_1+\tau_2}(\mathbf{x}, r, \mathbf{v}_0).$$

3.2. Brown-out Particle Model

In the following, we describe one particular particle model that is also governed by our generalized mass-dependent flow map. For our main test case, we used the brown-out particle model, described by Syal et al. [SGL10]. In the following we explain its essential components, i.e., the equations of motion, the sediment uplift and the splash entrainment, needed to simulate dust clouds around helicopters, yielding illustrations as in Figure 1. Fast particle simulations and subsequent visualizations can be of use to preview and steer parameters for long-term CFD simulations. In accordance with the current practice in CFD brown-out engineering [TKB12], we assume that particles do not affect the fluid.

3.2.1. Particle Motion

The equations of motion for particles in Stokes' flow are, as described by Crowe et al. [CST98]:

$$\frac{\mathrm{d}\mathbf{v}_p}{\mathrm{d}\tau} = \frac{\mathbf{u}(\mathbf{x}_p, t+\tau) - \mathbf{v}_p}{r_p} - \mathbf{g}, \tag{1}$$

whereas $\mathbf{x}_p$ is the particle's position, $\mathbf{v}_p$ its current velocity and r_p the particle response time, i.e., the time a particle needs to respond to a change in the flow velocity. The influence of the particle's mass on its trajectory is manifested in this response time r_p. (In fluid dynamics literature this parameter is usually named τ_p, but to avoid confusions with the integration duration, we rename it to r_p.) The particle response time simplifies for spherical particles in Stokes-type flows to (cf. Crowe et al. [CST98]):

$$r_p = \frac{\rho_p d_p^2}{18\nu} \tag{2}$$

Here, ρ_p is the density of a particle and d_p its diameter. If not mentioned otherwise we used for dry sand $\rho_p = 1600\ kg/m^3$. The kinematic viscosity is denoted as ν (in air $\nu = 1.81 \times 10^{-5}\ kg/(m\ s)$) and the gravity is denoted as $\mathbf{g}$ (with $g_y = -9.8065\ m/s^2$).

A common measure for the inertia of particles is the Stokes number S_k:

$$S_k = r_p / r_\eta, \tag{3}$$

with r_η being the Kolmogorov time scale [LMC92]. Particles with very low Stokes numbers ($S_k \ll 1$) are known to follow path lines of the flow closely. The Stokes number is proportional to the particle response time (Eq. (3)), thus if the response time approaches zero (i.e., due to zero mass, see Eq. (2)), a mass-less particle follows a path line. However, considering particles with very small mass in Crowe's equation (1) yields a singular perturbation problem. (See Haller and Sapsis [HS08] for a method to turn it into a regular perturbation problem in unsteady flows.)

We transform Eq. (1) into a formulation using the flow map $\phi = \phi_t^\tau(\mathbf{x}, r)$:

$$\frac{d\mathbf{v}_p}{d\tau} = \frac{d^2\phi}{d\tau^2} = \frac{\mathbf{u}(\phi, t+\tau) - \frac{d\phi}{d\tau}}{r_p} - \mathbf{g}. \tag{4}$$

We solve Eq. (4) using an explicit two-step Euler method with integration step size s for particles released from rest, i.e., $\mathbf{v}_0 = \mathbf{0}$ from the point $(\mathbf{x}_0, t_0)$:

$$\begin{aligned} \mathbf{x}_p' &= \mathbf{x}_p + s\,\mathbf{v}_p \\ t' &= t + s \\ \mathbf{v}_p' &= \mathbf{v}_p + s\left(\frac{\mathbf{u}(\mathbf{x}_p, t) - \mathbf{v}_p}{r} - \mathbf{g}\right). \end{aligned}$$

In addition to the implementation of the flow map ϕ (by Eq. (1)), further conditions and events are required to simulate brown-out, which are described in the following.

3.2.2. Uplift Threshold Velocity

Particles on the ground are subject to several forces. Due to drag and gravity (prevalent at large particles), and cohesive forces between particles (prevalent at small particles), a certain minimum lift force is required to aerodynamically entrain a particle from the ground. This threshold has been studied by a number of researchers [Bag41, GI85]. Conventionally, the friction velocity $v_\star$ is expressed as:

$$v_\star = \sqrt{w/\rho},$$

with w being the wall shear stress. The (far-field) flow density is denoted as ρ, which was set in the CFD simulation to be a constant of $\rho = 1.225\ kg/m^3$. Similar to Syal et al. [SGL10], we use the model of Shao and Lu [SL00] to express the minimum velocity required to entrain a particle:

$$v_{\star,t} = A\sqrt{\left(\frac{\rho_p - \rho}{\rho}||\mathbf{g}||\,d_p + \frac{\beta}{\rho\,d_p}\right)}, \tag{5}$$

where $A = 0.1109$ and $\beta = 3\times10^{-4}$ for aeolian flows. The uplift condition is $v_\star > v_{\star,t}$.

3.2.3. Splash Entrainment

A particle that hits the ground with a sufficiently large energy can entrain further particles, either when encountering a strong downwash flow in saltation or by convection due to the rotor disk, gaining relatively high velocity toward the sediment bed, cf. Shao and Li [SL99]. The kinetic energy injected by the impacting particle overcomes the bonding and cohesive forces of smaller, resting particles, therefore lifting them up, which is in sedimentology known as *splash entrainment*. After dislodging particles that rested on the ground the impacting particle rebounds and is further entrained by the flow. After the moment of impact the impacting particle undergoes three phases that are: compression, sliding (in which a Coulomb frictional force with coefficient f acts) and the recovery. According to Syal et al. [SGL10] the rebound velocity $\mathbf{d} = (d_x, d_y, d_z)^T$ of an impacting particle with velocity $\mathbf{v}_p = (v_x, v_y, v_z)^T$ is given as

$$\begin{aligned} d_x &= v_x + \varepsilon_x f(e+1)v_y \\ d_y &= -e v_y \\ d_z &= v_z + \varepsilon_z f(e+1)v_y, \end{aligned}$$

with ε_x and ε_z being the in-plane velocity components of the impacting particle. The coefficient of restitution e is defined as d_y/v_z for spherical particles. Shao and Lu [SL00] calculate the number of particles ejected from the ground N_s by an incoming particle with velocity $\mathbf{v}_p$ using:

$$N_s = \frac{c_s - 1.9a^2\left(1 - e^{\gamma||\mathbf{v}_p||}\right)}{2h^2}, \tag{6}$$

with $\gamma = 2$, $a = 0.6$, and $h = 0.08$. For the fraction of energy c_s that is not converted to heat we chose $c_s = 1$ (nothing is lost). Alike Syal et al. [SGL10], we modeled splash entrainment as a probabilistic process, i.e., we ejected particles with a normal distribution around the rebound velocity $\mathbf{d} = (d_x, d_y, d_z)^T$.

In Figure 2(a), we present a particle visualization that color-codes for each particle the event leading to the entrainment. It can be seen that splashing mainly occurs below the rotor disk and in the downwash flow behind the helicopter, which both correlates to the observations of Syal et al. [SGL10]. If splashed particles are small enough, they lift up (e.g., directly in front of the helicopter), otherwise they are dragged along on the ground (e.g., few meters ahead of helicopter). Furthermore, Syal et al. [SGL10] reported that small particles mainly lift up due to splash entrainment, since often the aerodynamic drag alone is not sufficient to overcome the cohesive forces. The size of the particles is color-coded in Figure 2(b), showing that uplifted splashed particles have indeed a smaller size.

4. Mass-dependent Integral Curves

The trajectories of mass-dependent particles are of great importance as the mass correlates to the energy and thereby the forces inflicted on rotorcrafts, causing deterioration or view limitations. In this section we introduce the four natural classes of integral curves for mass-dependent particles. For the advection of those curves we simplified the model of Syal [SGL10], only considering the equations of motion (i.e., the flow map), but not the rebounding and splash entrainment of additional lines, as they would rapidly consume the available memory, due to extensive refinement.

Mass-dependent Path Line. Using the mass-dependent flow map $\phi_t^\tau(\mathbf{x}, r)$, the trajectory of a mass-dependent particle – for brevity called *mass-dependent path line* – can be described as a parametric curve in the form:

$$\mathbf{p}(\tau) = \phi_t^\tau(\mathbf{x}, r),$$

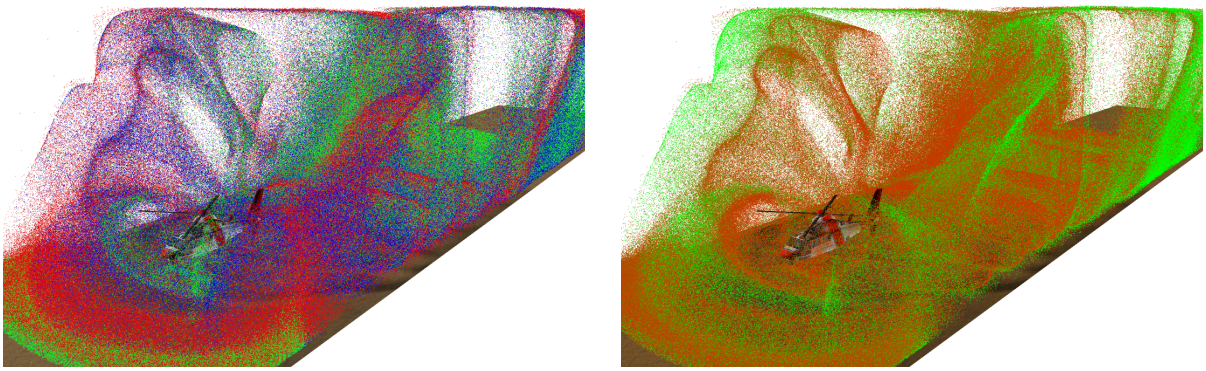

(a) Figure showing entrainment types of particles, which is either by uplifting (●), rebounding (●) or splashing (●).

(b) Color coding of the mass of particles, invoking brown-out conditions, for particles between $d_p = 10\mu m$ (●) and $d_p = 100\mu m$ (●).

Figure 2: *Insights on particles in brown-out simulations.*

when seeding at position $\mathbf{x}$ at time t with response time r. Such path lines can be used to visualize where particles of a certain mass are transported to over time. Figure 3(a) illustrates a mass-dependent path line in mass-space-time.

Mass-dependent Streak Line. The temporal coherence between particles of equal mass can be visualized by *mass-dependent streak lines* $\mathbf{s}(\tau)$, see Figure 3(b), which can be described using:

$$\mathbf{s}(\tau) = \phi_{\tau}^{t-\tau}(\mathbf{x}, r).$$

Mass-dependent Time Line. *Mass-dependent time lines* $\mathbf{t}(u)$ are used to reveal spatial coherent structures, as illustrated in Figure 3(c), and are defined as:

$$\mathbf{t}(u) = \phi_{t}^{\tau}(\mathbf{c}(u), r).$$

Mass Line. A new class of integral curves arises when varying the response time, while keeping the start location $\mathbf{x}$, start time t and integration duration τ constant. We name these curves *mass lines* and define them as:

$$\mathbf{m}(r) = \phi_{t}^{\tau}(\mathbf{x}, r)$$

These lines connect all locations that can be reached at a certain time $t + \tau$, starting from one place $\mathbf{x}$ by using different masses, i.e., the end points of mass-dependent path lines, see Figure 3(d). Since a path line and a streak line, seeded at the same position and time, share the end point, mass lines are also the connections of the end points of mass-dependent streak lines. (We examine an example in Section 6.) On a further note, the length of mass lines correlates with the separation introduced by particles released with different mass, which can be used as a descriptor for features. Similar to time lines, mass lines have the limitation to not directly visualize the correspondance to the seeding structure.

5. Implementation

The following section provides details on our GPU implementation and the employed techniques for the visualization.

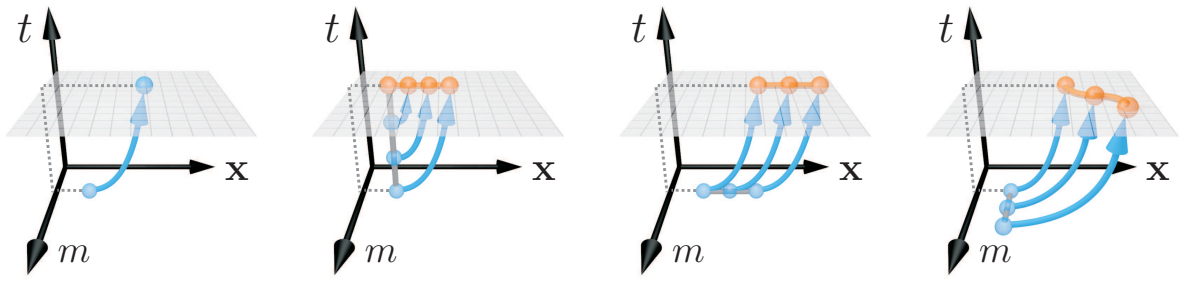

(a) Path line (●)

(b) Streak line (●)

(c) Time line (●)

(d) Mass line (●)

Figure 3: *Illustrations of the integral lines in mass-space-time.*

5.1. Integral Geometry

The particles and the integral curves are both integrated on the GPU using geometry shaders, at a step size of at most 0.116 ms. The capability of the geometry shader to dynamically insert vertex data is of use for the splash entrainment of further particles and the adaptive refinement of the integral curves. Syal et al. [SGL10] detected more small particles in the flow than large particles. Therefore, we randomly choose the mass for the particle to entrain between a minimum mass and the mass of the impacting particle. We compute the number of splashing particles according to Eq. (6) to compute the energy correctly, but only emit a single particle at a custom probability. This ensures that the number of particles entrained and simulated is controllable, so that we can avoid overflows of the stream output buffers. (Correct densities can be computed by modeling the emission as Monte Carlo sampling, i.e., particles carry weights according to their selection probability.) Streak, time and mass lines are refined dependent on the edge lengths. We chose the refinement scheme that is most commonly used on GPUs, i.e., to emit a new particle in the center of the edge that needs refinement. Unsteady vector field data often exceeds the video memory, which is why we asynchronously stream the data of the next time steps to a ring buffer on the GPU.

5.2. Visualization

In Figure 1 particles were rendered as viewport-aligned quads, expanded in the geometry shader. They were shaded with ISL shading by Zöckler et al. [ZSH96] and received shadows by using Fourier opacity mapping (FOM) of Jansen and Bavoil [JB10]. For the FOM we used 7 coefficients, stored at a resolution of 512^2 and used weighted average blending as proposed by Bavoil and Myers [BM08] for the composition of the transparent particles. Integral lines were shaded with ISL shading, too. Depth cues were added by depth-dependent halos of Everts et al. [EBRI09]. As a frame of reference we placed an Eurocopter AS365 Dauphin helicopter in the brown-out scenes. (The CFD simulation only contained the rotor disk, not this particular model.)

6. Applications

In this section, we apply the integral curves to three data sets, one analytic and two real-world. Furthermore, we present measurements of the performance of our interactive GPU implementation, captured in the helicopter data set.

6.1. Beads Flow

We investigated an analytic field, namely an unsteady 2D biofluid dynamic model known from Wiebel et al.'s [WCW*09] investigation of its vortex core. We used an analytic approximation of this vector field, named Beads flow, as given by Weinkauf and Theisel [WT10], which was originally provided by Ronald Peikert. Path lines, streak lines and mass lines are shown for this data set in space-time in Figure 4. As illustrated, mass lines connect the end points of both path and streak lines, seeded with varying mass, see Figure 4(a). Releasing path lines with continuously increasing mass assembles a surface. Furthermore, we show an example for the mass-dependence of topological structures, such as vortex cores, in Figure 4(b). While heavy particles diverge due to inertia, light particles can converge to a mass-dependent core line. The smaller the mass, the closer the mass-less path line core, reported by Weinkauf and Theisel [WT10], is approached. It can be seen that the mass-dependent particle model is coherent with traditional mass-less particles when approaching zero mass (for zero gravity).

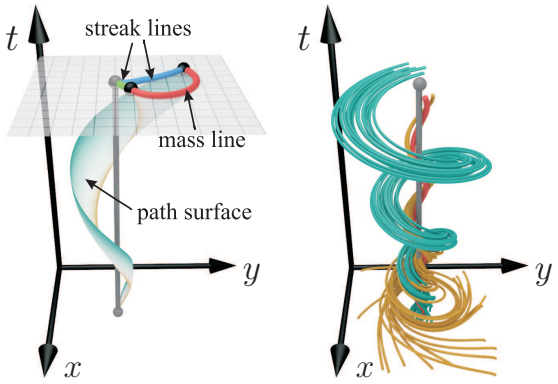

(a) The mass line (●) connects the end points of both path lines ($d_p = 15\mu m$ (●) to $500\mu m$ (●)) and streak lines ($d_p = 15\mu m$ (●), $500\mu m$ (●)).

(b) Converging and diverging mass-dependent path lines ($d_p = 15\mu m$ (●), $500\mu m$ (●)) and the mass-less path line core (●), reported in [WT10].

Figure 4: *Integral lines in the Beads flow, depicted in space-time. Gravity is set to zero.*

6.2. Helicopter in Ground Proximity

We illustrated brown-out conditions around a helicopter in slow forward flight close to the ground, as one of the authors of this paper is a domain expert in this field. The data set we used is described in [KKKK12] and is a validated simulation in a wind tunnel (test case No. 12 in the paper), computed in about $4\frac{1}{2}$ weeks wall clock time on 256 processors on the cray cluster at the High Performance Computing Center in Stuttgart, Germany. We uniformly resampled 400° rotor revolution at 10° per time step at a resolution of $700 \times 100 \times 130$ voxels, yielding in total 4.2 GB of vector field data. In Figure 5 the trajectories of mass-dependent particles are shown for different masses. Not only do the trajectories change when modifying the mass (e.g., due to drag and gravity), but also does the number of entrained particles vary due to the uplift threshold $v_\star, t$, see Eq. (5). In Figure 6

streak lines of different mass are shown. Note that the vortex in front of the helicopter uplifts smaller particles directly (Fig. 6(a)), whereas larger particles partially fall back to the ground and bounce off (Fig. 6(c)). Especially, to the left and right of the helicopter the vortex that traps the sand particles is highly unsteady and requires much refinement of the lines. Figure 7 uses time lines to makes the influence of the mass apparent. Smaller particles are more subject to the unsteadiness of the vector field, thereby exhibiting more turbulent behavior. Figure 8 depicts mass lines in the helicopter data set. Therefore, the response time is varied, which is either achieved by a change of the diameter, the particle's density or the viscosity. Eitherway, the same line is acquired, but with a different parameterization and other meaning. Modifying the diameter allows to observe the separation of differently sized particles, while a variation of the density allows to view differences between dry and moist sand. Throughout the paper, we kept the density and kinematic viscosity constant.

Our domain experts confirmed three use cases, in which the mass lines in Figure 8 are of particular help. When rotorcrafts approach the ground, personnel is exposed to forceful air blows, possibly causing injuries. Mass lines visualize for multiple sizes simultaneously in which directions particles are tossed and also what the critical sizes are that lead to uplift, giving leads which areas to avoid when rotorcrafts approach. (In the case of slow forward flight, a few meters in the frontal hemisphere.)

The second application concerns the rotor blades. Mass lines depict which particles of a certain mass spectrum enter the rotor disk, causing blade erosion and mechanical wear. Figure 8 shows that nearly the whole spectrum of masses enters the rotor from the frontal left and frontal right direction, as viewed from the pilot.

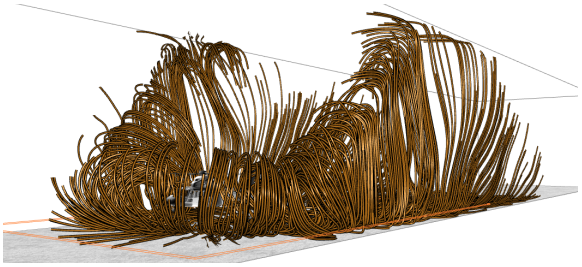

(a) Mass-dependent path lines, $d_p = 15\mu m$

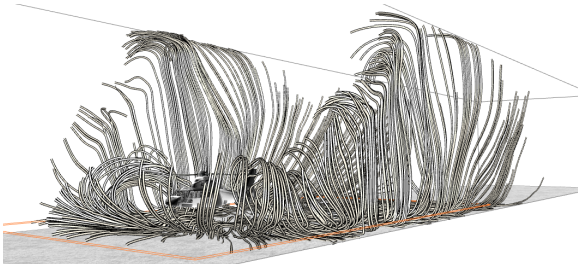

(b) Mass-dependent path lines, $d_p = 50\mu m$

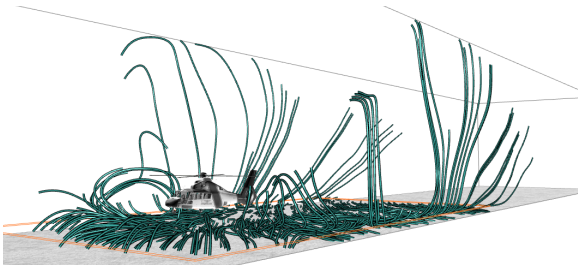

(c) Mass-dependent path lines, $d_p = 90\mu m$

Figure 5: *Depictions of path lines with different mass in the helicopter data set. Larger particles do not lift as high, due to gravity.*

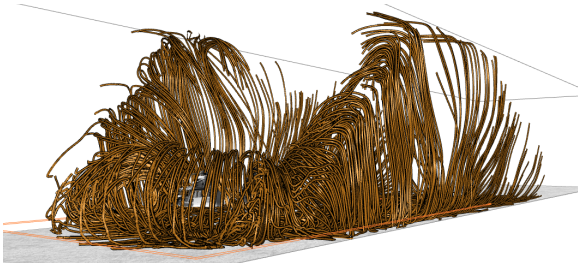

(a) Mass-dependent streak lines, $d_p = 15\mu m$

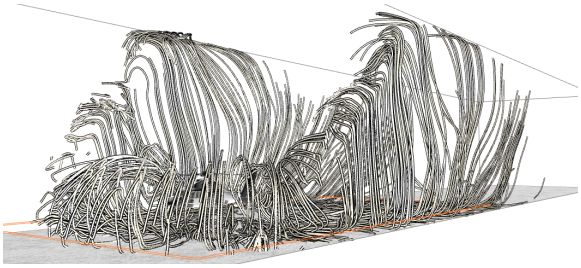

(b) Mass-dependent streak lines, $d_p = 50\mu m$

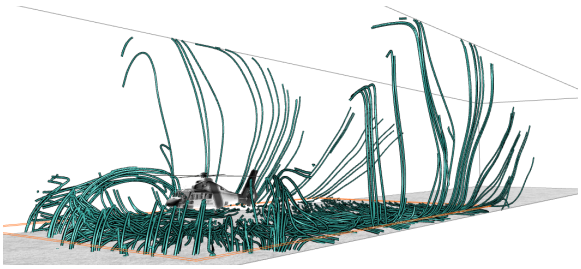

(c) Mass-dependent streak lines, $d_p = 90\mu m$

Figure 6: *Depictions of streak lines with different mass in the helicopter data set. A higher uplift threshold and gravity keep larger particles closer to the ground.*

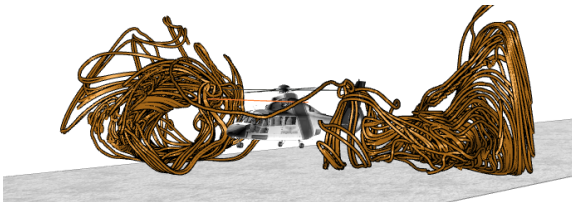

(a) Mass-dependent time line, $d_p = 15\mu m$

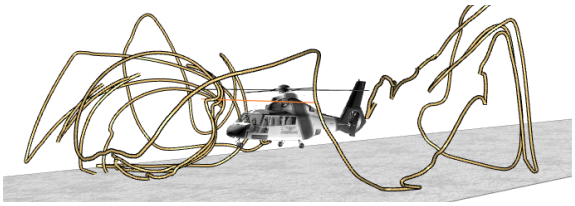

(b) Mass-dependent time line, $d_p = 30\mu m$

Figure 7: *Time lines seeded below the rotor disk reveal that lighter particles are more subject to turbulence.*

The third use case is called modified saltation bombardment and is concerned with particles that return to the sediment bed after a short uplift due to a nearby vortex. These impacting particles entrain smaller particles, thereby contributing to brown-out. The mass lines in Figure 8 show masses that take part (which is dependent on the distance to the vortex), e.g., directly in front of the helicopter lower masses (i.e., smaller particles) fall back to the sediment bed than on the frontal left and right.

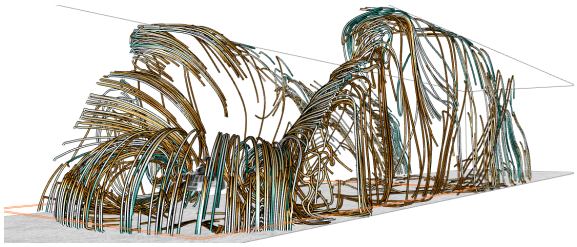

Figure 8: *Depiction of mass lines with a varying diameter $d_p = 10\mu m..100\mu m$, color-coded from brown (●) to teal (●).*

6.3. Hydrocyclone

Another example for the information conveyed by mass lines is shown in Figure 9 in a steady hydrocyclone data set, which was provided by Markus Rütten (and was uniformly resampled to $256 \times 369 \times 536$ voxels). Here, the particle model does neither include aerodynamic nor splash entrainment, but a particle-boundary interaction, i.e., the reflection of particles at the wall geometry. The employed particle model cannot yet describe interactions between different media, but gives reasonable results when observing the paths of only few particles (neglecting inter-particle forces). The mass-dependence of the particle trajectories is expressed by swirling mass lines. The fact that they expand leads to the conclusion that particles with different mass exit the bottleneck after a different time. This is also visible when comparing the path line images, in which lighter particles exit the bottleneck later, since they circled the bottleneck longer.

(a) Path lines with particle diameters of $15\mu m$ (●), $25\mu m$ (●), $35\mu m$ (●) and $50\mu m$ (●).

(b) Mass lines ($d_p = 15..50\mu m$)

Figure 9: *Hydrocyclones are used to separate particles in liquid suspensions based on density variations. As visible in Fig. 9(a), an increase of mass (and thereby inertia) causes particles to drift off the vortex core and to exit at different times. Mass lines in Fig. 9(b) expand and swirl around the bottleneck, which shows that lighter particles reside longer in the bottleneck.*

Table 1: *Timings for the simulation of 2 million mass-dependent particles, captured in the helicopter data set (17 fps), as in Fig. 1.*

Pipeline step	Time per frame
Particle integration	12.3 ms
FOM construction	15.9 ms
Particle rendering	22.8 ms

Table 2: *Timings for the interactive integration of 2k intergral lines in the helicopter data set. ($d_p = 15\mu m$, for mass lines $d_p = 15..100\mu m$)*

Pipeline step	Path	Streak	Time	Mass
Integration	1.2 ms	3.9 ms	3.4 ms	1.0 ms
Rendering	2.7 ms	6.0 ms	6.3 ms	1.7 ms
Total fps	202	100	92	340

6.4. Performance

For all measurements we used a machine equipped with an Intel Core I7-2600K CPU with 3.4 GHz and an Nvidia Quadro 6000 GPU with 6GB VRAM. All images were rendered at a resolution of 1280×916 pixels with $16\times$ coverage-sampling anti-aliasing (CSAA). The performance of the particle simulation is shown in Table 1. Dependent on the fillrate, 10-19 frames per second (fps) are obtained for 2 million mass-dependent particles. For the individual classes of intergral curves the performance is measured in Table 2. Due to the absence of refinement, path lines are fast to integrate and render on the GPU. Streak lines and time lines adaptively generate more line geometry, which slows down integration and rendering (by factor 2). Mass lines were shorter than the other line classes, therefore less geometry was created, which made both the integration and the rendering faster. Coincidentally, mass lines produced less occlusion. Summarizing, direct particle visualizations usually require a high number of individual particles to reveal structures in the flow. The integral lines presented in this work, however, are a fast and compact alternative that can furthermore reveal temporal and spatial coherence, as well as mass separation.

7. Conclusion

In this paper we extended geometry-based flow visualization tools, usually used in mass-less particle-based visualizations, to mass-dependent particles. We defined a new flow map to abstract the application-dependent particle model, i.e., the assumptions made in the equations of motion. Based on that, we derived four classes of mass-dependent integral curves in unsteady vector fields: path lines, streak lines, time lines, and a new class called *mass lines* that visualizes the separation of particles with different response times, i.e., due to different size or density. We demonstrated the influence of the mass in particle-based visualizations and used the integral geometry in an artificial and two real-world data sets. Hereby, our main test case was the brown-out simulation around a helicopter flying forward in ground proximity.

The processes involved in brown-out are not yet fully understood, since it is difficult and expensive to validate the models, cf. Syal et al. [SGL10]. This is where we see much potential for future work, e.g., in the assistance in model validation, interactive previews for parameter steering of the long-term simulations, and most importantly, capturing the behavior of particles with mass in unsteady flow and revealing structures, e.g., vortices carrying heavy particles. But brown-out simulations are just one application of mass-dependent particle visualization techniques. Furthermore, we plan to assist in examining arterial plaque in hemodynamic flows, potentially causing cardiac infarcts. On a further note, mass-dependent topology is a promising field of research.

References

[Ang10] ANGILELLA J.-R.: Dust trapping in vortex pairs. *Physica D Nonlinear Phenomena 239* (Sept. 2010), 1789–1797. 2

[Bag41] BAGNOLD R.: *The Physics of Blown Sand and Desert Dunes.* Methuen, 1941. 4

[Bet37] BETZ A.: The ground effect on lifting propellers. *Zeitschrift für angewandte Mathematik und Mechanik 17*, 2 (April 1937). 2

[BFTW09] BÜRGER K., FERSTL F., THEISEL H., WESTERMANN R.: Interactive streak surface visualization on the GPU. *IEEE Transactions on Visualization and Computer Graphics (Proceedings Visualization / Information Visualization 2009) 15*, 6 (November-December 2009), 1259–1266. 2

[BM08] BAVOIL L., MYERS K.: *Order independent transparency with dual depth peeling*. Tech. rep., NVIDIA Research, 2008. 6

[CFK*10] CARTWRIGHT J., FEUDEL U., KÁROLYI G., MOURA A., PIRO O., TÉL T.: Dynamics of finite-size particles in chaotic fluid flows. In *Nonlinear Dynamics and Chaos: Advances and Perspectives*, Thiel M., Kurths J., Romano M. C., Károlyi G., Moura A., (Eds.), Understanding Complex Systems. Springer Berlin Heidelberg, 2010, pp. 51–87. 2

[CST98] CROWE C., SOMMERFIELD M., TSUJI Y.: *Multiphase Flows with Droplets and Particles*. CRC Press, 1998. 2, 3

[D'A10] D'ANDREA A.: Unsteady numerical simulations of helicopters and tiltrotors operating in sandy-desert environment. In *Proceedings of the American Helicopter Society Specialist's Conference on Aeromechanics* (January 2010). 2

[EBRI09] EVERTS M. H., BEKKER H., ROERDINK J. B. T. M., ISENBERG T.: Depth-dependent halos: Illustrative rendering of dense line data. *IEEE Transactions on Visualization and Computer Graphics 15* (November 2009), 1299–1306. 6

[Fra59] FRADENBURGH E. A.: The helicopter and the ground effect machine. In *Symposium on Ground Effect Phenomena* (October 1959). 2

[FW12] FRAEDRICH R., WESTERMANN R.: Motion visualization of large particle simulations. In *Proceedings of IS&T/SPIE*

Electronic Imaging 2012, Conference on Visualization and Data Analysis (2012), SPIE, pp. 82940Q–1 – 12. 2

[Gan06] GANESH B.: *Unsteady aerodynamics of rotorcraft at low advance ratios in ground effect*. PhD thesis, Georgia Institute of Technology, School of Aerospace Engineering, 2006. 2

[GI85] GREELEY R., IVERSEN J. D.: *Wind as a geological process on Earth, Mars, Venus and Titan.*, vol. 4 of *Cambridge Planetary Science Series*. Cambridge University Press, 1985. 4

[Hey60] HEYSON H. H.: *Ground effect for lifting rotors in forward flight*. NASA TN D-234, NASA, 1960. 2

[HS08] HALLER G., SAPSIS T.: Where do inertial particles go in fluid flows? *Physica D Nonlinear Phenomena 237* (May 2008), 573–583. 1, 2, 3

[HSW11] HLAWATSCH M., SADLO F., WEISKOPF D.: Hierarchical line integration. *IEEE Transactions on Visualization and Computer Graphics 17*, 8 (2011), 1148–1163. 2

[JB10] JANSEN J., BAVOIL L.: Fourier opacity mapping. In *Proceedings of the 2010 ACM SIGGRAPH symposium on Interactive 3D Graphics and Games* (New York, NY, USA, 2010), I3D '10, ACM, pp. 165–172. 6

[KKKK12] KUTZ B. M., KOWARSCH U., KESSLER M., KRÄMER E.: Numerical investigation of helicopter rotors in ground effect. In *30th AIAA Applied Aerodynamics Conference* (2012), no. AIAA-2012-2913 in 30. 6

[KKKW05] KRÜGER J., KIPFER P., KONDRATIEVA P., WESTERMANN R.: A particle system for interactive visualization of 3D flows. *IEEE Transactions on Visualization and Computer Graphics 11* (2005), 744–756. 2

[KLB10] KALRA T. S., LAKSHMINARAYAN V. K., BAEDER J. D.: CFD validation of micro hovering rotor in ground effect. In *Proceedings of the American Helicopter Society, 66th Annual Forum* (May 2010). 2

[KSW04] KIPFER P., SEGAL M., WESTERMANN R.: Uberflow: a GPU-based particle engine. In *Proceedings of the ACM SIGGRAPH/EUROGRAPHICS conference on Graphics hardware* (New York, NY, USA, 2004), HWWS '04, ACM, pp. 115–122. 2

[KSW*12] KARCH G. K., SADLO F., WEISKOPF D., MUNZ C.-D., ERTL T.: Visualization of advection-diffusion in unsteady fluid flow. *Computer Graphics Forum 31* (2012), 1105–1114. 2

[LLR08] LEE T. E., LEISHMAN J. G., RAMASAMY M.: Fluid dynamics of interacting blade tip vortices with a ground plane. In *Proceedings of the American Helicopter Society, 64th Annual Forum* (May 2008). 2

[LMC92] LANDAHL M. T., MOLLO-CHRISTENSEN E.: *Turbulence and random processes in fluid mechanics*. Cambridge University Press, 1992. 3

[LTH08] LI G.-S., TRICOCHE X., HANSEN C.: Physically-based Dye Advection for Flow Visualization. *Computer Graphics Forum 27*, 3 (2008), 727–734. 2

[MKW08] MAPES P., KENT R., WOOD R.: *DoD Helicopter Mishaps FY85-05: Findings and Recommendations*. Tech. rep., U.S. Air Force, 2008. 2

[MLP*09] MCLOUGHLIN T., LARAMEE R., PEIKERT R., POST F., CHEN M.: Over two decades of integration-based, geometric flow visualization. *Eurographics 2009, State of the Art Reports* (2009), 73–92. 1, 2

[Nat10] NATHAN N. D.: *The rotor wake in ground effect and its investigation in a wind tunnel*. PhD thesis, University of Glasgow, Faculty of Engineering, Department of Aerospace Engineering, 2010. 2

[NG12] NATHAN N. D., GREEN R. B.: The flow around a model helicopter main rotor in ground effect. *Experiments in Fluids 52* (2012), 151–166. 2

[PRN*11] PETERKA T., ROSS R., NOUANESENGSY B., LEE T.-Y., SHEN H.-W., KENDALL W., HUANG J.: A study of parallel particle tracing for steady-state and time-varying flow fields. In *Proceedings of the 2011 IEEE International Parallel & Distributed Processing Symposium* (Washington, DC, USA, 2011), IPDPS '11, IEEE Computer Society, pp. 580–591. 2

[Pul06] PULLA D. P.: *A study of helicopter aerodynamics in ground effect*. PhD thesis, The Ohio State University, 2006. 2

[SGHK03] SAIJO T., GANESH B., HUANG A., KOMERATH N. M.: Development of unsteadiness in a rotor wake in ground effect. In *AIAA 21st Applied Aeromdynamics Conference* (June 2003). 2

[SGL10] SYAL M., GOVINDARAJAN B., LEISHMAN J. G.: Mesoscale sediment tracking methodology to analyze brownout cloud developments. In *Proceedings of the American Helicopter Society, 66th Annual Forum* (2010). 1, 2, 3, 4, 6, 9

[Sha05] SHADDEN S. C.: Lagrangian coherent structures. http://mmae.iit.edu/shadden/LCS-tutorial/, 2005. 3

[SL99] SHAO Y., LI A.: Numerical modelling of saltation in the atmospheric surface layer. *Boundary-Layer Meteorology 91* (1999), 199–225. 4

[SL00] SHAO Y., LU H.: A simple expression for wind erosion threshold friction velocity. *Journal of Geophysical Research 105* (Sept. 2000), 22437–22444. 4

[TKB12] THOMAS S., KALRA T., BAEDER J.: A hybrid CFD methodology to model the two phase flowfield beneath a hovering laboratory scale rotor. *Proceedings of the 42nd AIAA Fluid Dynamics Converence* (June 2012). 3

[WCW*09] WIEBEL A., CHAN R., WOLF C., ROBITZKI A., STEVENS A., SCHEUERMANN G.: Topological flow structures in a mathematical model for rotation-mediated cell aggregation. *Topological Data Analysis and Visualization: Theory, Algorithms and Applications* (2009), 1–12. TopoInVis. 6

[WHT12] WEINKAUF T., HEGE H.-C., THEISEL H.: Advected tangent curves: A general scheme for characteristic curves of flow fields. *Computer Graphics Forum (Proc. Eurographics) 31*, 2 (May 2012), 825–834. CGF. 2

[WT10] WEINKAUF T., THEISEL H.: Streak lines as tangent curves of a derived vector field. *IEEE Transactions on Visualization and Computer Graphics (Proceedings Visualization 2010) 16*, 6 (November - December 2010), 1225–1234. Received the Vis 2010 Best Paper Award. 6

[WWSS10] WIEBEL A., WANG Q., SCHNEIDER D., SCHEUERMANN G.: Accelerated streak line computation using adaptive refinement. *Journal of WSCG 18* (2010), 17–23. 2

[XPP00] XIN H., PRASAD J., PETERS D. A.: An analysis of partial ground effect on the aerodynamics of a helicopter rotor. In *AIAA 38th Aerospace Sciences Meeting and Exhibit* (January 2000). 2

[Zbr47] ZBROZEK J.: *Ground effect on the lifting rotor*. R.A.E. Technical Note No. Aero. 1903 2347, Aeronautical Research Council, 1947. 2

[ZSH96] ZÖCKLER M., STALLING D., HEGE H.-C.: Interactive visualization of 3D-vector fields using illuminated stream lines. In *Proceedings of the 7th conference on Visualization '96* (Los Alamitos, CA, USA, 1996), VIS '96, IEEE Computer Society Press, pp. 107–ff. 6